

Histatin-1 is an endogenous ligand of the sigma-2 receptor

Kyung-No Son¹, Hyun Lee², Dhara Shah¹, Sushma Kalmodia¹, Ryan Cree Miller³, Marwan Ali¹, Arun Balasubramaniam¹, Stephanie M. Cologna⁴, Hyunjoon Kong³, Deepak Shukla¹ and Vinay Kumar Aakalu¹ 

¹ Department of Ophthalmology and Visual Sciences, University of Illinois at Chicago, IL, USA

² Department of Pharmaceutical Science and Biophysics Core at Research Resources Center, University of Illinois at Chicago, IL, USA

³ Department of Chemical & Biomolecular Engineering, University of Illinois at Urbana-Champaign, IL, USA

⁴ Department of Chemistry, University of Illinois at Chicago, IL, USA

Keywords

antimicrobial peptide; histatin-1; MAC30; migration; sigma-2 receptor; TMEM97; wound healing

Correspondence

V. K. Aakalu, Department of Ophthalmology and Visual Sciences, University of Illinois at Chicago, 1855 W. Taylor St., MC 648, Suite 3.158, Chicago, IL 60612, USA

Tel: 312-996-9120

E-mail: vaakalu@uic.edu

(Received 12 March 2021, revised 30 May 2021, accepted 11 June 2021)

doi:10.1111/febs.16108

The Sigma-2 receptor (S2R) (a.k.a TMEM97) is an important endoplasmic reticular protein involved in cancer, cholesterol processing, cell migration, and neurodegenerative diseases, including Niemann–Pick Type C. While several S2R pharmacologic agents have been discovered, its recent (2017) cloning has limited biological investigation, and no endogenous ligands of the S2R are known. Histatins are a family of endogenous antimicrobial peptides that have numerous important effects in multiple biological systems, including antifungal, antibacterial, cancer pathogenesis, immunomodulation, and wound healing. Histatin-1 (Hst1) has important roles in epithelial wound healing and cell migration, and is the primary wound healing agent in saliva. Little is understood about the downstream machinery that underpins the effects of histatins, and no mammalian receptor is known to date. In this study, we show, using biophysical methods and functional assays, that Hst1 is an endogenous ligand for S2R and that S2R is a mammalian receptor for Hst1.

Introduction

The Sigma-2 receptor (S2R) was recently identified as the endoplasmic reticular protein, Transmembrane Protein 97 (TMEM97) [1]. S2R, implicated heavily in cancer and neurodegenerative diseases, was originally described pharmacologically, with disparate small molecules and drugs found to target S2R. These agents are active in multiple areas including cancer, pain, Alzheimer's disease, aging and mitochondrial disorders, and multiple sclerosis [2]. TMEM97 is also known to be important in cancer cell metastasis, cellular migration and has a described interaction with the Niemann–Pick Type C (NPC) intracellular cholesterol transporter 1 (NPC1) protein [1,2]. NPC1 is deficient, or defective, in the vast majority of patients with

Niemann–Pick Type C disease, and is critical for cholesterol processing and distribution [3–5]. While numerous actions and pharmacologic modulators have been tied to TMEM97/S2R, to our knowledge, no well-described endogenous ligand is known [1,2].

Belonging to the endogenous antimicrobial peptide (AMP) family, histatins were originally thought to be antifungal components of saliva [6]. In the last decade, numerous roles for histatins have been described in multiple epithelial and nonepithelial systems, including antiviral, antibacterial, wound healing, and immunomodulatory actions [7–9]. Histatins, particularly histatin-1 (Hst1), are thought to be the primary wound healing agents in saliva and are known to promote cell migration and

Abbreviations

(NPC1) protein, NPC intracellular cholesterol transporter 1; AMP, antimicrobial peptide; CD, circular dichroism; DTG, 1,3-di-*o*-tolylguanidine; EMT, epithelial–mesenchymal transition; GPCR, G protein–coupled receptor; HCE, human corneal epithelial; Hst1, Histatin-1; Hst3, histatin-3; KD, knockdown; NPC, Niemann–Pick Type C; S2R, sigma-2 receptor; SP, scrambled peptide; SPR, surface plasmon resonance; TMEM97, transmembrane protein 97.

modulate cellular adhesion in multiple cell types [7–9]. Histatins are overexpressed in multiple cancer cell types and may modulate the effects of epithelial-mesenchymal transition (EMT) factors in these cancers [9–12]. Although there has been interest in finding the receptor for histatin peptides, limited information has been described. Imamura *et al.* reported on the ability of histatin-3 (Hst3) to interact with, but not clearly directly bind, the chaperone protein HSC70. No other mammalian cellular interactors are known to explain the cell migration and wound healing effects of Hst1 [13,14]. Other clues to a potential receptor include the sensitivity of the effects of histatins to pertussis toxin application, suggesting at least a downstream functional role of a G protein-coupled receptor (GPCR) [7–9].

Given our interest in histatins, we undertook a receptor screening assay to search for a receptor for histatin peptides. This screening assay identified TMEM97 as a putative partner for Hst1. We utilized multiple methods in vetting this interaction, including radioligand binding, coimmunoprecipitation, ELISA assay, direct binding analysis using surface plasmon resonance (SPR), circular dichroism (CD), immunolocalization, and functional assays to validate Hst1 as a binding partner of TMEM97, and identify an endogenous secreted ligand for TMEM97. All of these experiments described herein established TMEM97 as a mammalian histatin receptor. Moreover, we demonstrate that the pro-migratory effects of Hst1 are abrogated by knockdown (KD) of TMEM97. These results have broad importance to understanding how histatins promote cellular migration, identifying an endogenous ligand for TMEM97, and improving our understanding of wound healing and cellular migration.

Results

Hst1 Binds TMEM97

Screening for potential receptors for Hst1 was carried out at the University of North Carolina (UNC) Psychoactive Drug Screening Program (PDSP) using radioligand binding assays on an existing library of overexpressed cell lines of various pharmacologically important receptors. Binding of synthetic Hst1 with TMEM97 containing HEK293T membranes was identified in a primary binding screen at 10 μ M of Hst1 and confirmed with a secondary dose-response binding assay using the same radioligand. Results were compared with a reference inhibitor, haloperidol, over a range of doses as described [15], and overlaid dose-response curves of the confirmatory radioligand binding

assay test are shown in Fig. 1A. The determined K_i value of the Hst1 was 239 nM, while that of haloperidol was 44 nM. This encouraging Hst1 K_i value motivated us to design and carry out further validation assays.

We then performed a coimmunoprecipitation assay to determine whether the potential interaction between Hst1 and TMEM97 was reproducible at the cellular level. After exogenous application of Hst1 to human corneal epithelial (HCE) cells, cell lysates were obtained and immunoprecipitation with a TMEM97 antibody followed by immunoblotting with an Hst1 antibody demonstrated that Hst1 was coprecipitated with TMEM97 (Fig. 1B). Interestingly, two bands (one below 10 kDa and one just below 15 kDa) were noted on co-IP. These bands may represent monomeric and multimeric versions of Hst1 and are similar to what has been seen with western blotting of Hst1 containing samples in the past [16]. These results suggest that the cell-free findings of this interaction (radioligand binding assay in cell membrane preparations) are demonstrable in the physiologic cellular environment. These results were confirmed with Hst1 antibody immunoprecipitation and blotting with anti-TMEM97 antibody (Fig. S1). In addition, proteomic analysis was performed using the gel fragment taken from the co-IP (precipitated with anti-Hst1 and blotted with anti-TMEM97) and confirmed the presence of TMEM97 (data not shown). Enzyme-linked immunosorbent assay (ELISA) testing to detect bound Hst1 on plates coated with TMEM97 was also performed and confirmed binding between Hst1 and TMEM97 (Fig. 2).

Both the radioligand binding assay and co-IP were done in cellular environments with other cellular components present with the possibility of having some other mediating partners. Hence, we investigated direct binding analysis of Hst1 with purified recombinant TMEM97 proteins *in vitro* using the SPR technique. SPR testing was performed with the highly sensitive SPR instrument Biacore 8K and demonstrated that Hst1 selectively bound to full-length TMEM97, which was expressed in a eukaryotic system (HEK293 cells; Fig. 1C). Subsequent testing with a GST-tagged, wheat germ-derived, C-terminal domain of TMEM97 (108–176) determined that Hst1 bound to the C-terminal region of TMEM97 with similar binding affinity as the full-length protein (Fig. 1E). As shown in Table 1, Hst1 contains many charged residues, which could cause nonspecific charge-charge interactions even though 150 mM salt was present in the SPR binding buffer to reduce this potential nonspecific interaction. A scrambled peptide control version of Hst1, Hst1-scrambled peptide (SP), contains the exact same amino acid residues as Hst1 but with different order. Hst1SP

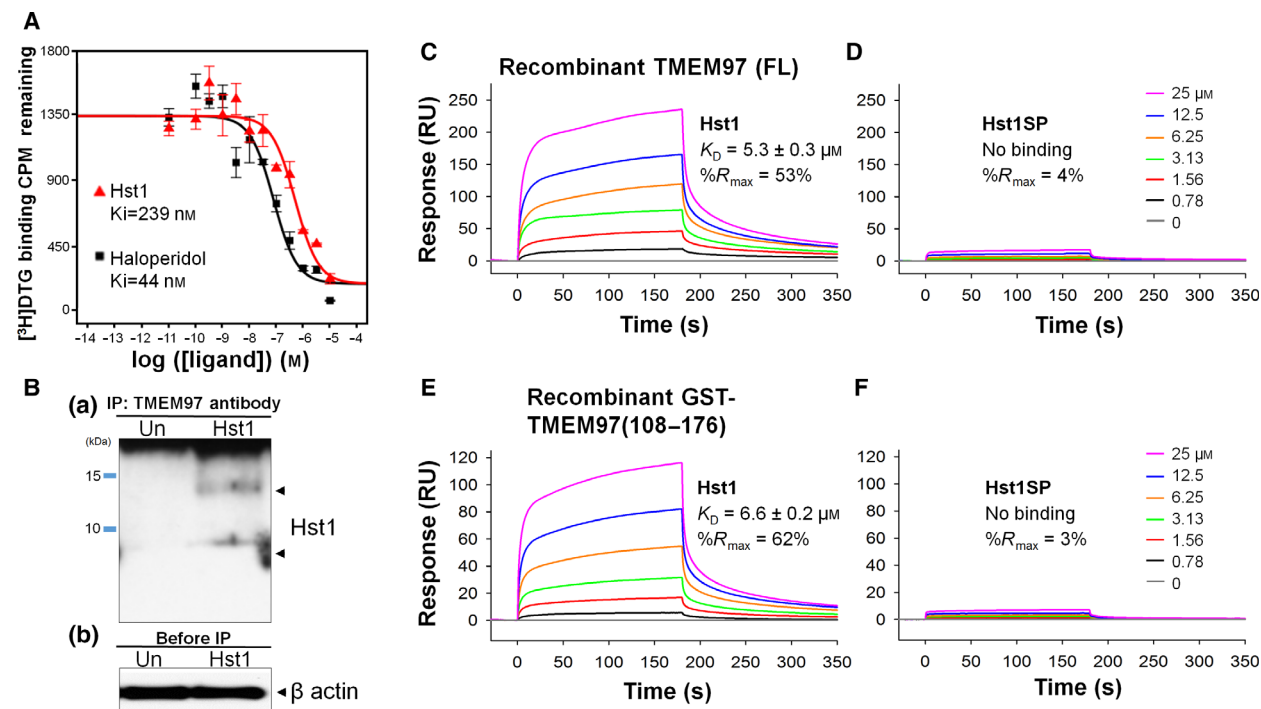


Fig. 1. Identification of TMEM97 as a potential Hst1 receptor. (A) Radioligand binding assay demonstrates that Hst1 binds to TMEM97. Binding affinity of Hst1 to TMEM97 was determined using HEK293T cell membranes with overexpression of TMEM97. Hst1 demonstrated a K_i of 239 nm as opposed to reference inhibitor haloperidol ($K_i = 44$ nm), indicating the pharmacologic relevance of this novel potential interaction. Experiments were performed in triplicate in three separate experiments. CPM = counts per minute. Error bars indicate SEM. (B) Hst1 coimmunoprecipitates with TMEM97. Hst1 was applied exogenously to HCE cells followed by immune precipitation with a TMEM97 antibody and subsequent immunoblotting with an Hst1 antibody. Images are representative of two separate experiments. Results indicate that Hst1 and TMEM97 are able to interact in physiological cellular environments. Un = Untreated sample. (C–F) Surface plasmon resonance (SPR) analysis demonstrates direct, specific binding between Hst1 and TMEM97. Sensorgrams of recombinant TMEM97 (FL) binding to a series of increasing concentrations of Hst1 (C) and scrambled peptide control (Hst1SP) (D). Sensorgrams of recombinant GST-TMEM97 (108–176) binding to Hst1 (E) and Hst1SP (F). These results indicate Hst1 can bind to FL-TMEM97 or its C terminus with similar affinities and that Hst1SP is unable to bind either recombinant form of TMEM97. K_D values were calculated from two rate constants determined by fitting the data (see Methods for details) with 1 to 1 Langmuir kinetic model, and the average K_D values and the standard deviations were calculated from 2 to 4 different experiments.

did not exhibit binding to either full-length TMEM97 or TMEM97 (108–176; Fig. 1D,F), indicating the observed binding interaction between Hst1 and TMEM97 was unlikely to be derived by nonspecific charge–charge interactions. These results suggest that there is a specific and direct binding of Hst1 with the C-terminal domain of TMEM97.

Subsequently, we generated synthetic C-terminal TMEM97 (108–176) and found that C-terminal synthetic TMEM97 (108–176) bound Hst1 with similar affinity to full-length and GST-tagged recombinant TMEM97 (108–176; Fig. 2A). As expected, Hst1SP did not bind to the synthetic TMEM97 (108–176; Fig. S3). In order to compare side by side, overlaid steady-state affinity fitting curves of Hst1 binding to a full-length TMEM97 (black), a GST-TMEM97(108–176) (red) and a synthetic TMEM97(108–176) (green) are shown in

Fig. 2B), and their determined K_D values are 5.3, 6.6 and 6.3 μM , respectively. We then tested the hypothesis that interaction between Hst1 and TMEM97 could affect their structures upon binding. We examined the secondary structure of Hst1, Hst1SP, and TMEM97 (108–176) in solution using CD measurements (Fig. 2C). We noted that Hst1 and scrambled Hst1SP alone are mostly disordered (over 50%) with some degree of β -strand (light and dark blue lines, respectively, in Fig. 2C, while TMEM97 (108–176) contains mainly α -helical (46%) and 23% β -strand regions with ~31% disordered (14% turns and 17% unordered) regions (Fig. 2D). According to CD spectra comparison (pink line vs black line), there appeared to be slightly more α -helical secondary structures formed upon Hst1 binding to TMEM97 (108–176) than TMEM97 (108–176) alone, reducing turns region from 14% to 8% while β -strand

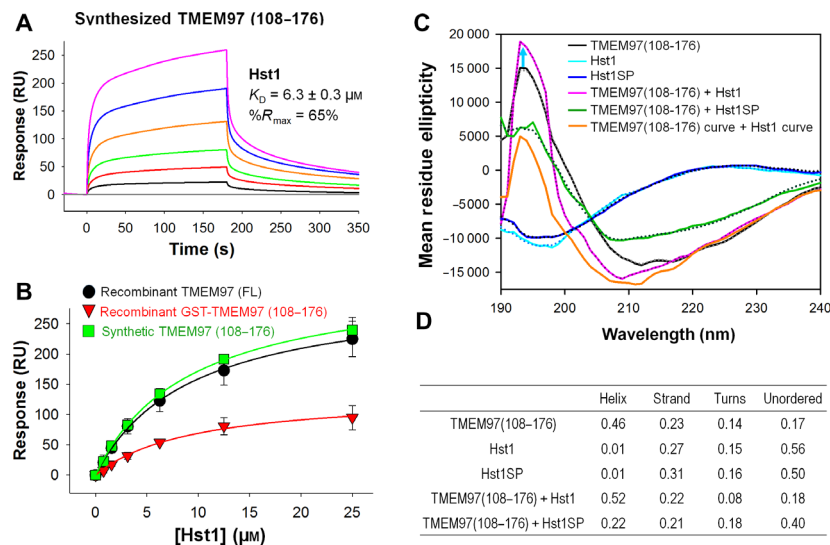


Fig. 2. Direct binding analysis by surface plasmon resonance (SPR) and secondary structure analysis using circular dichroism (CD). SPR analysis demonstrates binding of Hst1 with synthetically generated C-terminal domain TMEM97 (108-176). (A) Sensorgrams of synthetic TMEM97 (108-176) binding to Hst1. (B) Overlaid steady-state affinity fitting curves of Hst1 binding to full-length TMEM97 (black), GST-TMEM97 (108-176) (red) and synthetic TMEM97 (108-176) (green). Results indicate that Hst1 can bind to synthetic C-terminal domain of TMEM97 with similar affinities to recombinant FL and C-terminal TMEM97. K_D values were calculated from two rate constants determined by fitting the data (see Methods for details) with 1 to 1 Langmuir kinetic model, and the average K_D values and the standard deviations were calculated from two to four different experiments. K_D values determined from steady-state affinity fittings were very similar to those from kinetic fittings. (C–D) Hst1 binding to TMEM97 increases secondary structures in both. CD spectrum of Hst1 (light blue line) or Hst1SP (dark blue line) alone shows equal to or over 50% of disordered pattern while TMEM97 alone (black line) CD data demonstrates that it is 46% α -helix and 23% β -strand region. Mixture of TMEM97 and Hst1 in solution reduces turn regions and increases helical configuration (pink line) as compared with each alone. Moreover, combining Hst1SP and TMEM97 (green line) did not induce increased secondary structural features. These results suggest that TMEM97 and Hst1 binding can induce further secondary structures in solution. Each sample was run in duplicate, and CD data analysis was done on DichroWeb Data Analysis. Dotted lines are the fitted lines.

Table 1. Sequences of synthetic TMEM97, Hst1 and Hst1SP used in experimentation

Name	Sequence
TMEM97 (108-176)	MTTLIPILSTFLFEDFSKASGFKGQRPETLHER LTLVSVYAPYLLIPFILLIFMLRSPYYKY EEKRKKK
Histatin-1 (Hst1)	D _p SHEKRHHGYRRKFHEKHHSHREFPFYGDYGS NYLYDN
Hst1SP	HYHKFHRYYDPGSNLKEHNHGFHHGYKDE FRRE _p SRDS

and unordered regions remain similar. The scrambled peptide Hst1SP did not induce increased secondary structural elements, unlike Hst1 (green line in Fig. 2C). Simple sum (orange line) of CD spectra of TMEM97 (108-176) alone and Hst1 alone was demonstrably different from Hst1 bound to TMEM97 (108-176). CD data analysis using DichorWeb revealed that disordered regions (turns plus unordered) of the Hst1-TMEM97 (108-176) complex are lower than each of them alone. These results suggested that not only does Hst1 bind to

TMEM97, but the interaction may further induce secondary structures.

Hst1 and TMEM97 co-localize in cellular environments

In order to determine whether the binding assay results were relevant to normal cellular conditions and function, we performed several assays to confirm the existence and relevance of an interaction between Hst1 and TMEM97. We tested whether Hst1 could be internalized into HCE cells and whether localization of internalized Hst1 could colocalize with TMEM97. Figure 3A demonstrates the results of these experiments. Alexa-488 coupled synthetic Hst1 was applied exogenously and noted to be internalized into HCE cells at 24 h after exposure, with relative enrichment of localization to the peri-nuclear area. Subsequent immunolocalization of exogenously applied Hst1 to HCE cells and visualization with an ER staining agent demonstrated good colocalization (Fig. 3B). Finally, coimmunolocalization of exogenously applied Hst1 with TMEM97 demonstrated

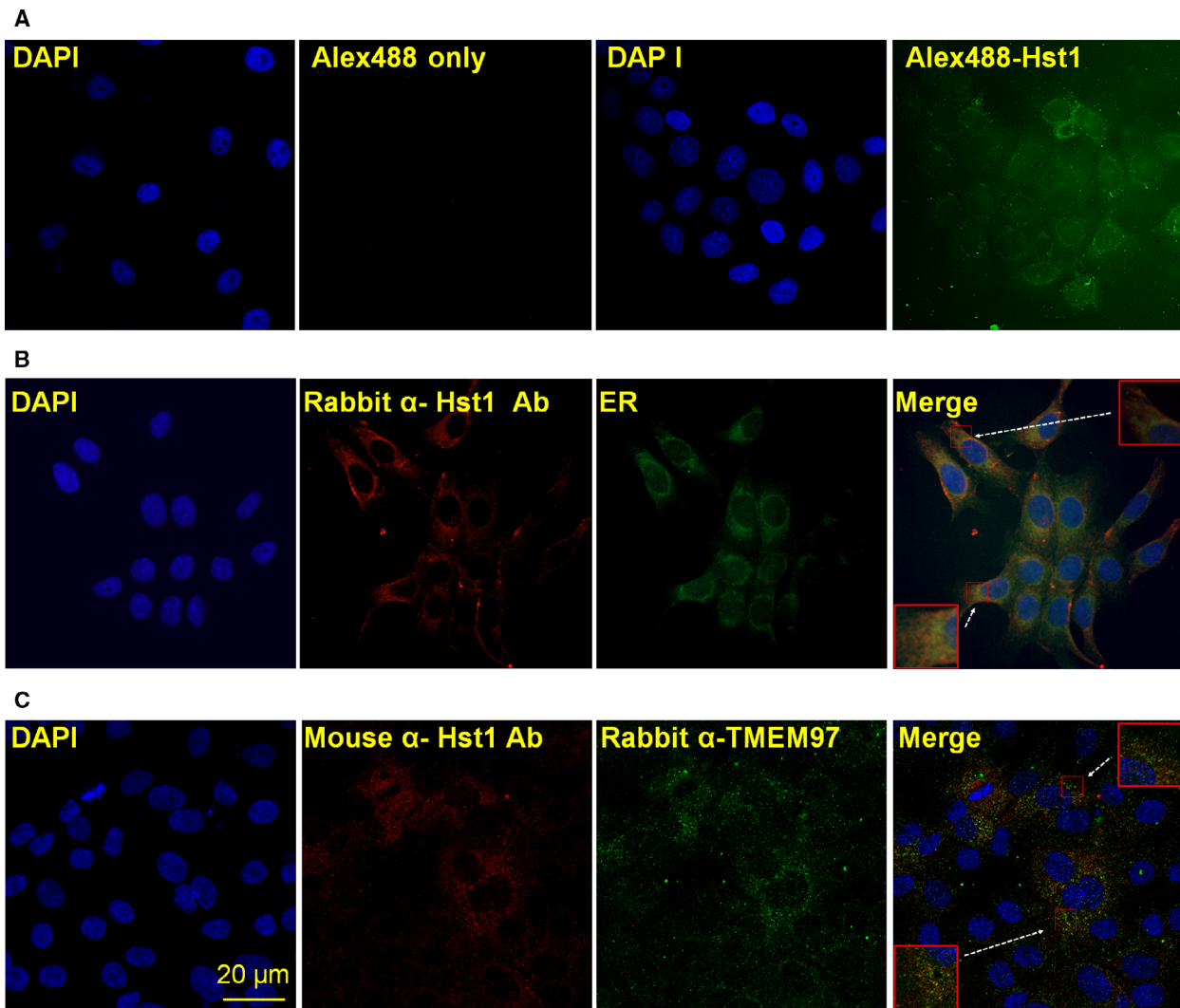


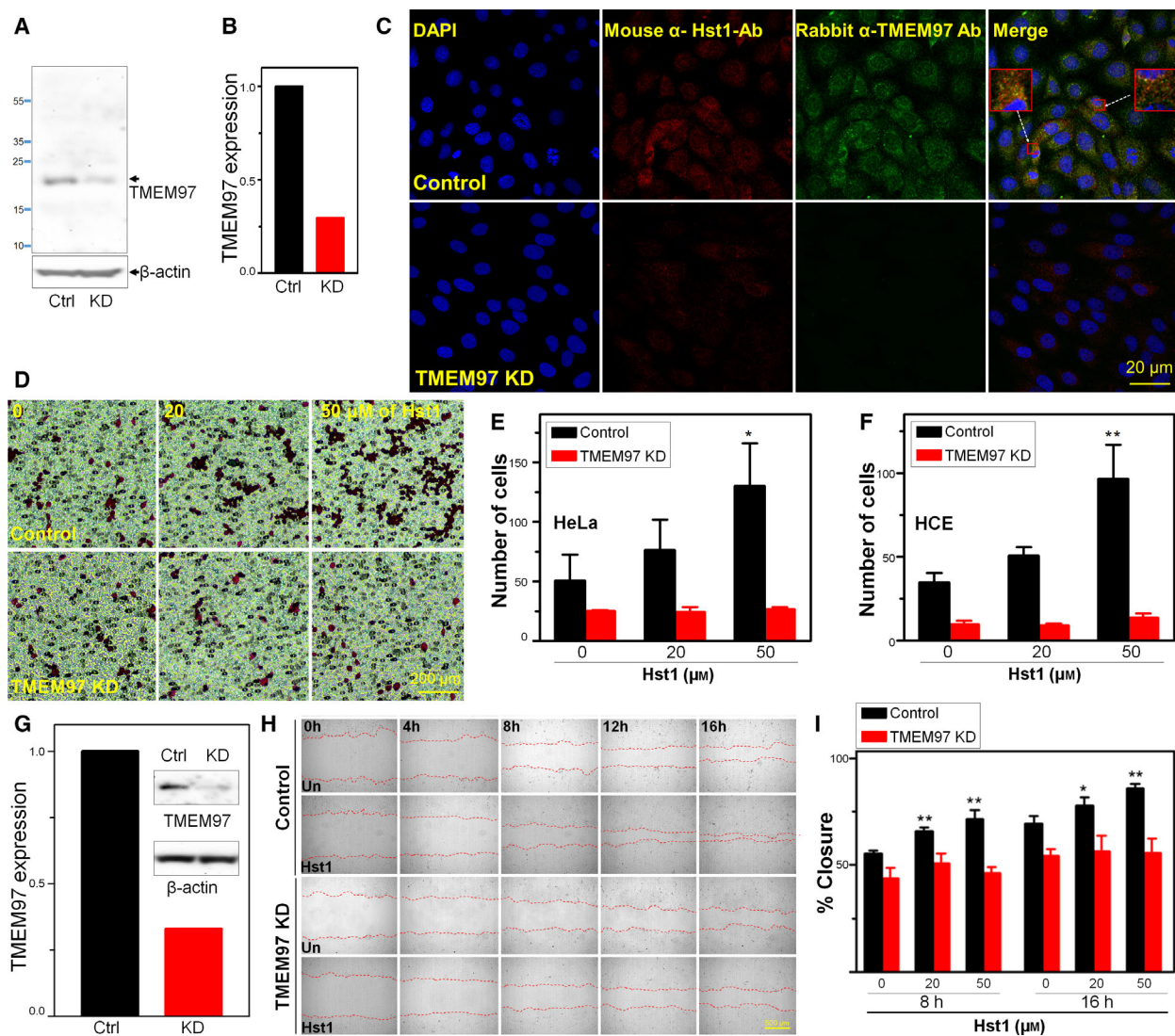
Fig. 3. Hst1 colocalizes with TMEM97 at the endoplasmic reticulum (ER). (A) Hst1 is internalized by epithelial cells and localizes to the peri-nuclear area. Confocal microscopic imaging of HCE cells 24 h after exposure to exogenous Alexa-488 coupled Hst1 demonstrates internalization of Hst1 into cells and relative enrichment of localization to the peri-nuclear area. (B) Hst1 localizes to the endoplasmic reticulum (ER). Exogenously applied Hst1 was immunolocalized with a rabbit anti-Hst1 antibody and colocalizes with an ER visualization agent (Cytopainter ER staining kit; Abcam). (C) Colocalization of exogenously applied Hst1 with intrinsic ER protein TMEM97. Exogenously applied Hst1 was visualized with a mouse anti-Hst1 antibody and colocalizes with signal from a rabbit anti-TMEM97 antibody. Taken together, these findings indicate that colocation of Hst1 and TMEM97 is demonstrable in normal cellular environments and that this interaction occurs at predicted cellular sites of TMEM97 function. Scale bar = 20 μ m. Images are representative of three separate experiments.

significant overlap (Fig. 3C). These results suggest that Hst1 is localized to the area where TMEM97 is thought to have a functional role and that the previously described binding assays may have a physiological correlate in live cells. In addition, we performed Hst1 localization by immunofluorescence after exogenous application of Hst1 in cells pretreated with escalating concentrations of 1,3-di-*o*-tolylguanidine (DTG) and noted that Hst1 localization is reduced by pretreatment

with DTG, correlating well with radioligand binding assay results (Fig. S4).

TMEM97 is required for migration promotion by Hst1

Testing was then performed to determine whether the known functions of Hst1 on HCE or HeLa cells were dependent upon TMEM97 expression, including cell



migration and wound healing. In order to assess the importance of TMEM97 in the known functions of Hst1, we performed a siRNA KD of TMEM97 in HCE and HeLa cells (Fig. 4). Internalization and localization of Hst1 in KD cells versus control cells were then tested (Fig. 4C). Notably, KD of TMEM97 significantly disrupted internalization and/or localization of Hst1 in HCE KD cells. Boyden chamber-based cell migration assays were performed in HCE and HeLa cells with and without siRNA KD of TMEM97 and demonstrated that, as predicted, Hst1 treatment caused a dose-dependent increase in cellular transmigration toward a stimulus (2% FBS). KD of TMEM97 in HCE and HeLa cells abolished this response to Hst1, suggesting that transmigration acceleration in response to Hst1 is

dependent upon the presence of TMEM97 (Fig. 4D–F). Subsequently, we tested whether Hst1-dependent increases in wound healing of HCE cells, using a standard scratch assay, were dependent upon TMEM97. In order to do this, we generated a shRNA KD of TMEM97 in HCE cells (Fig. 4G). Similarly, we noted the predicted increases in wound healing rates in response to Hst1 in HCE cells and shRNA KD of TMEM97 abolished this responsiveness (Fig. 4H–I). Figure S5 demonstrates a similar necessity of TMEM97 in HCE cells to increase rates of scratch closure in response to Hst1 using a siRNA-mediated KD. As the mechanism for Hst1 induced wound healing and epithelial cell migration has been the subject of much study and is still unknown, this finding suggests a novel potential pathway/mechanism for this phenomenon.

Fig. 4. Knockdown (KD) of TMEM97 inhibits Hst1 induced migration and wound healing. (A) HCE cells were transfected for 48h with either control siRNA (Ctrl) or TMEM97 siRNA [knockdown (KD)]. Whole cell lysates were then subjected to western blotting with antibodies against TMEM97. (B) Densitometry measurements indicate that TMEM97KD reduced protein levels by 70%. Notable is the significant reduction in TMEM97 signal in the TMEM97 siRNA treated samples indicating successful KD. (C) Immunolocalization shows internalization of Hst1 to HCE and colocalization with TMEM97 in the perinuclear/ER area with control siRNA transfection and loss of both TMEM97 signal and loss of internalized Hst1 signal in KD cells, suggesting that TMEM97 is either necessary for internalization or localization of Hst1. Scale bar = 20 μ m. Images are representative of three separate experiments. (D–F) Boyden chamber migration assay testing for response of HeLa and HCE cells to migrate across a membrane toward FBS in response to treatment with Hst1. Control siRNA transfected cells increase transmigration in a dose-dependent manner in response to Hst1 exposure. This responsiveness to Hst1 is lost in TMEM97 KD cells, highlighting the importance of TMEM97 for this action of Hst1. (D) Images of Boyden chamber membranes showing HeLa cells stained with Eosin. Scale bar = 200 μ m. (E–F) Cell counting of transmigrated cells (E = HeLa, F = HCE) in the Boyden chamber assay with and without KD of TMEM97 over a range of concentrations of Hst1. Notable is the loss of Hst1 responsiveness in both cell types after KD of TMEM97. Statistical significance was determined by 2-way ANOVA with Bonferroni's *post hoc* test. ** P < 0.01. Error bars indicate Standard Error of the Mean. Experiments were performed in triplicate. Statistical analyses were performed using GRAPHPAD PRISM software 5.0 (GraphPad Software, La Jolla, CA, USA). (G–I) Wound healing experiment testing necessity of TMEM97 for Hst1 responsiveness. (G) shRNA mediated KD of TMEM97 in HCE cells was tested using western blotting for TMEM97 protein comparing control and KD cells. Densitometry measurements indicate that shRNA KD reduced protein levels of TMEM97 by 70%. (H) Time lapse microscopy [Image Express Micro (Molecular Devices, CA, USA)] at 4x magnification, after standardized wounding of confluent HCE cells in serum free conditions, was used to quantify migration rates and scratch closure times with and without Hst1 cotreatment at the time of wounding, with and without TMEM97 KD. Scale bar = 500 μ m. (I) Bar graph depicting scratch closure % over time. Notably, we found a statistically significant improvement in scratch closure rates (versus untreated control) with Hst1 treatment (20 or 50 μ m) of concentrations at 8 and 16 h and loss of this response to Hst1 application in the TMEM97 KD cells. Statistical significance was determined by 1-way ANOVA with Bonferroni's *post hoc* test. * P < 0.05; ** P < 0.01. Error bars indicate Standard Error of the Mean. Experiments were performed in triplicate. Statistical analyses were performed using GRAPHPAD PRISM software 5.0 (GraphPad Software, La Jolla, CA, USA). Taken together these results suggest that KD of TMEM97 can cause loss of Hst1 internalization or localization in HCE cells. Moreover, TMEM97 appears to be necessary for increases in HCE and HeLa cell migration and HCE scratch closure in response to Hst1.

Discussion

This study represents the demonstration of an endogenous ligand for TMEM97 and a mammalian receptor for Hst1. We discovered this novel ligand–receptor relationship through radioligand binding assay screening and confirmed these results by multiple different biochemical/biophysical methods of measuring protein–protein interaction. We also confirmed the necessity of TMEM97 for the wound healing activity of Hst1 peptides and found potential domains for interaction between these two proteins. These results may impact understanding of processes including wound healing, cholesterol processing, pathogen processing, and mucosal immunity.

TMEM97 was recently reported to be the elusive S2R [1]. S2R is the target of numerous pharmacologic ligands and is targeted for multiple purposes including cancer, schizophrenia, Alzheimer's disease, aging and mitochondrial disorders, and multiple sclerosis [2]. TMEM97 is an intrinsic ER protein involved in cholesterol and lysosomal processing that has been implicated in cell migration and interacts with NPC cholesterol transporter 1 protein, NPC1 [1,2]. NPC1 is critically important in cholesterol processing, pathogen processing, autophagy, and apoptosis [3–5]. Reduction of TMEM97 levels in NPC1 mutant cells leads to relative

normalization of free cholesterol levels, a critical feature of NPC disease, suggesting a therapeutic role for modulation at the TMEM97 protein for NPC disease [17].

S2R targeting agents have also been implicated in migration, caspase-mediated apoptosis, autophagy, reactive oxygen species generation, and mitochondrial stability [2]. One of the most important effects of the S2R/TMEM97/MAC30 is the promotion of cell migration and association with malignancies [18–22]. TMEM97 up- and downregulation has been seen in multiple tumor types, with upregulation seen in many cancers, and downregulation seen in renal and pancreatic cancers [23]. Interestingly, changes in cancer cell motility, invasiveness, and deregulation of epithelial-mesenchymal transition markers have been seen with derangement of TMEM97 levels [18,19,23,24]. While multiple actions and pharmacologic modulators have been tied to TMEM97/S2R and great importance has been placed on TMEM97, no endogenous ligand is known [1,2].

Histatins are an important class of endogenous AMPs. Other exemplary AMPs include LL-37 and β -defensins [6]. Histatin peptides are a histidine-rich family of peptides, arising from two genes (HTN1 and HTN3). Histatins were first described as antifungal agents in the saliva, but have since been found to have antiviral, antibacterial, wound healing, and even anti-inflammatory activities [7–9]. Histatins, particularly

Hst1 are thought to be the primary wound healing agents in the oral mucosa and promote cell migration and modulate cellular adhesion in epithelial, stromal, and vascular endothelial cells [7–9]. Migration induced by Hst1 in some cell types may involve endosomal protein recruitment and MAP kinase signaling changes [7–9]. Interestingly, it was recently reported that Hst1 is readily taken up into human buccal epithelial carcinoma cells and localized to the ER and mitochondria [25].

Histatins may be overexpressed in several cancer cell types and may modulate effects of EMT factors in some cancer cell types [9–12]. Moreover, a number of antimicrobial peptides genes (HTN1, HTN3, STATH, MUC7), with similar chromosomal localization (chr 4; 4q13.3) are seen to be significantly overexpressed in the peri-tumor area in papillary thyroid cancer samples, suggesting some potential interaction of these AMPs with cancerous lesions [26]. Hst5 also has sequence homology with CCL28 a chemokine with antimicrobial activity that has been tested as an adjuvant for HIV1 vaccine development and is upregulated in multiple cancers [27].

While Imamura *et al.* have reported on the ability of Hst3 to interact with, but not clearly directly bind, the chaperone protein HSC70, no other mammalian cellular interactors are known to explain the migratory effects of Hst1 [13,14]. Interestingly, HSC70 may be a modulator of NPC and levels of HSP70/HSC70 contributing to stabilization or destabilization of NPC1 levels [28].

Other clues to a potential interaction among histatins, TMEM97, and NPC1 are also seen in disparate reports of these previously unassociated proteins being involved in viral processing, infectivity, and invasion. HIV1 infected patients have been reported to have decreased Hst5 levels and increases in *Candida albicans* infections [9,29]. Moreover, NPC1 has been identified as the Ebola virus receptor. The common tie among these observations could be the importance of cholesterol processing in many viral infections [30].

While we believe it is exciting and impactful to identify an endogenous receptor for Hst1 and an endogenous ligand for TMEM97, it is not yet clear whether all of the actions of histatin peptides are explained by an interaction with TMEM97, or whether all the actions of TMEM97 are driven by histatins. It is possible that the associations of both of these proteins with phenotypic cellular changes are contextual and depend on tissue type, environmental conditions or other factors. This study does not answer whether a GPCR still exists to underpin some actions of histatin peptides and whether such a receptor is up or downstream of TMEM97. Finally, the interaction we describe could

be one of the multiple interactions, and future experiments are still needed to solve the structures of TMEM97 and Hst1 alone and together.

In conclusion, Hst1 is an endogenous ligand for TMEM97 and TMEM97 is a mammalian receptor for Hst1. Moreover, TMEM97 is necessary for transduction of the epithelial migration promoting effects of Hst1. These results help to resolve the search for an Hst1 receptor and broaden our understanding of physiological interactors for TMEM97. Implications for these findings may be found in our understanding of cholesterol processing, NPC disease, wound healing, and cell migration.

Materials and methods

Peptide synthesis

Hst1, Hst1-scrambled peptide (Hst1SP) and TMEM97 (108–176) peptides were synthesized according to previously published protocols [31]. Briefly, standard solid-phase peptide synthesis was carried out using Fmoc-based solid-phase peptide synthesis chemistry followed by purification using reversed-phase HPLC and subsequent characterization by electrospray ionization mass spectrometry. Table 1 shows the sequences of the synthetic peptides used in experiments.

Radioligand binding assay

Radioligand binding/competition assays were performed by the University of North Carolina (UNC) Psychoactive Drug Screening Program (PDSP) as described [15]. An S2R transient overexpression HEK293T cell line was used for membrane preparations. Primary and secondary radioligand binding assays were then performed using an initial 10 μ M concentration of Hst1 followed by determination of equilibrium binding affinity over multiple concentrations, in triplicate. The 'hot ligand' for S2R was [3 H]-1,3-di-o-tolylguanidine ([3 H]-DTG) and haloperidol was used as the prototypical inhibitor. Calculations of the percentage inhibition for each assay plate with total binding (with buffer) as 0% inhibition and nonspecific binding (in the presence of the reference compound) as 100% inhibition over an average of 4 experiments are used to identify whether the compound is suitable for secondary screening (> 50% inhibition). Secondary screening results are reported as amount of hot ligand binding [counts per minute (CPM)] remaining with a standard reference dose-response curve (all in triplicate). Determination of K_i 's for the reference drug (haloperidol) and the experimental article (Hst1) is then performed. Secondary screening assays are performed three separate times with three technical replicates for each experiment. Further details are available in the PDSP assay manual [32].

Cell culture

Human corneal epithelial (HCE) cells were provided by Deepak Shukla (University of Illinois at Chicago, Chicago, IL, USA). HCE cells were cultured in a Medium Essential Media (MEM) (10-010-CV, Corning, Cellgro, Manassas, VA, USA) supplemented with 10% Fetal Bovine Serum [(FBS), 26140-079, Gibco Life Technologies, Grand Island, NY, USA] and 1% penicillin- as reported prior [33,34]. Standard cell culture conditions (37 °C, 5% CO₂, > 95% humidity) were used during routine passages, as has been done previously [35]. HeLa cells were maintained in Dulbecco's modified Eagle's medium (DMEM; Life Technologies, Grand Island, NY, USA), and media were supplemented with 10% fetal bovine serum (FBS; Gibco/Life Technologies, Carlsbad, CA, USA) and 1% penicillin-streptomycin (Gibco/Life Technologies, Carlsbad, CA, USA).

Immunoprecipitation/western blotting

The day before, HCE cells were plated at the concentration of 5 x 10⁶ cells/well in a 100 mm dish and were treated with 20 μM of Hst1 for 6 h. Cells were harvested with lysis buffer (1% NP40, 137 mM sodium chloride, 20 mM Tris [pH 8.0], and 10% glycerol) and the lysates were incubated with 5 μL of a validated rabbit polyclonal anti-TMEM97 antibody (NBP1-30436, Novus Bio., Littleton, CO, USA) overnight at 4 °C [36]. The lysates were incubated with 30 μL of a suspension of protein A/G (sc-2003, Santa Cruz Biotechnology, Dallas, TX, USA) for 2 h at 4 °C with gently shaking. After centrifugation for 5 min, pellets were washed three times and resuspended in 50 μL of 2X NuPAGE LDS sample buffer (NP10007, Invitrogen, Carlsbad, CA, USA) and boiled for 10 min. For detecting bounded Hst1 to TMEM97 protein, the lysates were subjected to electrophoresis on 12% NuPAGE bis-Tris gels (NP0342BOX, Invitrogen, Carlsbad, CA, USA), followed by transfer to nitrocellulose membranes (Amersham Protran, GE Healthcare, Pittsburgh, PA, USA). Membranes were then blocked with Tris-buffered saline containing 3% nonfat dry milk for 1 h and incubated with rabbit primary antibody against Hst1 (MBS2002621, Mybiosource, San Diego, CA, USA; 1 : 1000) overnight at 4 °C [16]. After washing in 0.05% Tris-buffered saline containing 0.05% Tween 20 (TBST), membranes were then incubated for 1 h with goat anti-rabbit-HRP (BD Biosciences, San Jose, CA, USA; 1 : 2000) as the secondary antibody. The membranes were developed using MYELC Imager (Thermo Fisher Sci. Waltham, MA, USA) and ECL Pro solution (PerkinElmer, Waltham, MA, USA). β-actin was used as an internal control. For immunoprecipitation detection by mass spectrometry, the eluant was proteolytically digested using suspension trapping (S-Trap, ProtiFi, Farmingdale, NY, USA) and protein identification was carried out using nanoLC-MS on a Q-Exactive mass spectrometer as previously

described [37]. Protein identifications at the 95% confidence interval with a minimum of two unique peptides were considered.

Surface plasmon resonance (SPR)

Recombinant full-length TMEM97 (also called MAC30) and GST-TMEM97 (108-176) proteins were purchased from OriGene and Abnova, respectively (recombinant Full-length TMEM97 (TP316927, OriGene, Rockville, MD, USA) from HEK293 cells; recombinant GST-C-terminal TMEM97 (108-176, H00027346, Abnova, Taipei City, Taiwan, ROC from wheat germ). TMEM97 (108-176) peptide was synthesized. Two proteins and a peptide were initially prepared in HBS buffer containing [10 mM HEPES, pH 7.4, 150 mM NaCl, and 0.05% n-dodecyl-β-D-maltoside (DDM)]. DDM is known to be an effective membrane protein stabilizing detergent [38–40]. The CM5 sensor chip surface was first activated by 1-ethyl-3-(3-dimethylaminopropyl) carbodiimide hydrochloride (EDC)/N-hydroxy succinimide (NHS) mixture using a Biacore 8K instrument (Cytiva). Two recombinant proteins, full-length TMEM97 and GST-TMEM97 (108-176), were diluted to 50 μg·mL⁻¹ in 10 mM sodium acetate at pH 5.5 and immobilized to flow channels 1 and 2 followed by ethanolamine blocking on the unoccupied surface area. Synthesized peptide TMEM97 (108-176) was diluted to 50 μg·mL⁻¹ in 10 mM sodium acetate at pH 4.0 and immobilized to flow channel 3 on the same sensor chip. Each flow channel has its own reference channel, and blank immobilization using EDC/NHS and ethanolamine was done for all reference channels. Histatin solutions with a series of increasing concentrations (0.78–25 μM at twofold dilution) were applied to all four channels at a 30 μL·min⁻¹ flow rate at 25 °C. The data were double-referenced with a reference channel and zero concentration responses, and reference subtracted sensorgrams were fitted with 1 to 1 Langmuir kinetic model using a Biacore Insight evaluation software, producing two rate constants (k_a and k_d). The equilibrium dissociation constants (KD) were determined from two rate constants ($K_D = k_d/k_a$). For steady-state affinity fittings, response units at each concentration were measured during the equilibration phase, and the K_D values were determined by fitting the data to a single rectangular hyperbolic curve equation (1), where y is the response, y_{\max} is the maximum response and x is the histatin concentration.

$$y = \frac{y_{\max} \cdot x}{K_D + x} \quad (1)$$

Circular dichroism (CD)

CD analysis was performed on a Jasco 815 CD spectrometer at room temperature. Synthetic TMEM 97 (108-176) and two Hst1 peptides (Hst1 and Hst1SP) were prepared as

10 mM stock in 25% DMSO/water and water, respectively, and diluted to 0.15 mg·mL⁻¹ final concentration in CD buffer [10 mM Na₃HPO₄, pH 7.4, 0.05% n-dodecyl- β -D-maltoside (DDM, 89903, Thermo Fisher Sci. Waltham, MA, USA)]. A total of 400 μ L of each sample was added into a 1 mM quartz sample cell, and CD spectra were recorded from 260 nm to 190 nm wavelength. Data points were measured in 0.5 nm wavelength step at a scanning speed of 100 nm·min⁻¹. A total of 5 spectra were acquired for each sample and averaged. CD buffer without histatin peptides was used as a control curve, which was subsequently subtracted from the CD spectra of peptide samples. The resulting buffer control subtracted CD intensity row data in millidegrees were submitted to DichroWeb (<http://dichroweb.cryst.bbk.ac.uk>) and fitted with multiple embedded models and converted to mean residue ellipticity.

Immunofluorescence imaging

HCE cells were seeded on glass coverslips (Fisher Scientific Co., Pittsburgh, PA, USA) within a 6-well plate at 3 x 10⁵ (cells/well) seeding density. The cells were washed with media and were treated 20 μ M of Hst1 or untreated, both with reduced serum conditions (0.5% FBS in MEM media) for 6 h. HCE cells were then fixed in 3.7% paraformaldehyde, permeabilized with phosphate-buffered saline (PBS) containing 0.2% Triton X-100 for 5 min, and washed three times for 5 min each time in PBS. For blocking, cells were and incubated at room temperature for 30 min with 5% bovine serum albumin (BSA) and 5% normal goat serum in PBS. For the Endoplasmic Reticulum (ER) staining, a Cytopainter ER staining kit (ab139481, Abcam, Cambridge, MA, USA) was used, following the manufacturer's instructions. After washing with 1X Assay buffer, cells were incubated with Green Detection Reagent to cover the monolayer of cells. For the detection of Hst1 and TMEM97, mouse anti-Hst1 antibody (ab 70024, Abcam, Cambridge, MA, USA), rabbit primary antibody against Hst1 (MBS2002621, Mybiosource, San Diego, CA, USA, and rabbit anti-TMEM97 antibody (NBP1-30436, Novus Bio., Littleton, CO, USA) were used [16,36]. Cells were incubated overnight at 4 °C with primary antibodies, washed three times for 5 min each time in PBS before incubation with secondary antibodies for 30 min. Cells were then counterstained with 1 μ g·mL⁻¹ 4',6-diamidino-2-phenylindole (DAPI) solution in PBS for 3 min, then washed three times with PBS containing 0.05% Triton X-100 for 5 min each time, twice with PBS for 5 min each time, and once with distilled H₂O for 10 s. The cells were mounted in Fluoro gel with Tris buffer (Electron Microscopy Sciences, Hatfield, PA, USA) and observed under a confocal microscope (Zeiss LSM 710 Confocal Microscope, Oberkochen, Germany) using a 40x objective. Alexa FluorTM 488 NHS Ester (A20000, molecular probes, Carlsbad, CA, USA) was used for making Alexa-488 coupled synthetic Hst1.

Transfection/ knockdown of TMEM97

Sub-confluent monolayers of HCE or HeLa cells grown in 35-mm six-well plates were transfected with reaction mixtures consisting of 100 pmol of a pool of 3 target-specific 19–25 nt human small interfering RNAs (siRNA) to TMEM97 (sc-93890, Santa Cruz Biotechnology, Dallas, TX, USA) for 48 h and 5 μ L of Lipofectamine 2000 (11668027, Invitrogen, Carlsbad, CA, USA) in Opti-MEM media (31985-070, Gibco Life Technologies, Grand Island, NY, USA). Complexes were incubated for 20 min at 24 °C and then added to cells at 37 °C. Incubation was continued for 24–48 h at 37 °C in 5% CO₂. For the stable cell line KD of TMEM97, HCE was transfected with shRNA lentiviral particles to TMEM97 (sc-93890-V, Santa Cruz Biotechnology, Dallas, TX, USA) using polybrene (G062, Applied Biological Materials USA Inc. Ferndale, WA, USA) overnight. The next day, media was replaced with complete media without polybrene. After 48 h, transfected cells were selected using puromycin (1–10 μ g·mL⁻¹, A1113803, Gibco Life Technologies, Grand Island, NY, USA). KD of TMEM97 was confirmed with western blot using a rabbit anti-TMEM97 antibody (NBP1-30436, Novus Bio., Littleton, CO, USA) and analyzed by IMAGEJ software (ImageJ 1.47v, NIH, Thornwood, Bethesda, MD, USA).

Cell migration assay

HCE migration assays were performed in a 48-well microchemotaxis chamber (Neuro Probe, Inc., Cabin John, MD, USA), following the manufacturer's instructions and a modification of prior reports [41]. Polyester membranes (PFB12, Neuro Probe, Inc., Gaithersburg, MD, USA) with 12 μ m pores were used. HCE and HeLa cells were incubated with Hst1 for 6 h, harvested using Versene (15040-066, Life Technologies, Corp., Grand Island, NY, USA), resuspended in RPMI1640 (11875-093, Life Technologies, Corp., Grand Island, NY, USA) containing 0.5% FBS. The bottom chamber was loaded with RPMI1640 media containing 2% FBS, and the filter was laid over the media. The upper chamber was loaded with 3 x 10⁴ cells and then incubated at 37 °C for 16 h. The filters were then fixed and stained using Eosin (71311, Richard-Allan Sci., Kalamazoo, MI, USA). Each condition was studied in triplicate wells, and each experiment was performed three separate times, with three replicates from a single experiment depicted in figures.

Wound healing in vitro scratch assay

HCE cells were cultured in a 96-well plate at 5 x 10⁴ (cells/well) seeding density and were grown to confluence. Subsequently, a straight line scratch mark was made with a multi-scratch wound maker (Incucyte[®] 96-well Woundmaker Tool # 4563, Essen Biosciences, Ann Arbor, MI, USA). The cells were then washed twice with PBS to remove cellular debris. Wounded areas were then treated with or without 20 or

50 μ M of Hst1 in reduced serum conditions (0.5% FBS). Scratches were photographed microscopically at 4x magnification (Image express Micro, Molecular devices, San Jose, CA, USA) every hour over the course of the experiment. The wound areas were measured using ImageJ software (ImageJ 1.47v, NIH, Thornwood, Bethesda, MD, USA). Relative wound closure was calculated by dividing the closure of the treated wound by that of the untreated control wound. Each condition was studied in triplicate wells, and each experiment was performed three separate times, with three replicates from a single experiment depicted in figures.

Statistical analysis

All experiments were analyzed using standard statistical methods (Student's *t*-test, ANOVA), with the application of methods for multiple comparisons where appropriate using GRAPHPAD PRISM software 5.0 (GraphPad Software, La Jolla, CA, USA).

Acknowledgements

Portions of this work were carried out in the Protein Core and Biophysics Core of the Research Resources Center at the University of Illinois at Chicago. Special thanks to Lasanthi Jayathilaka PhD for her peptide synthesis expertise. Additional thanks to Melissa R. Peragine for work on the proteomics analysis. *Ki* determinations and receptor binding profiles were generously provided by the National Institute of Mental Health's Psychoactive Drug Screening Program (PDSP), Contract # HHSN-271-2018-00023-C (NIMH PDSP). The NIMH PDSP is directed by Bryan L. Roth MD, PhD at the University of North Carolina at Chapel Hill and Project Officer Jamie Driscoll at NIMH, Bethesda MD, USA. VKA acknowledges grant funding from: (a) National Eye Institute, NIH (USA): K08EY024339, R01EY029409, P30EY001792. (b) Department of Defense (USA): W81XWH-17-1-0122. (c) Veterans Affairs Office of Research and Development (USA): I01BX004080. (d) Research to Prevent Blindness, New York, NY (USA). DS acknowledges grant funding from: (a) National Eye Institute, NIH (USA) P30EY001792, R01EY024710. (b) Research to Prevent Blindness, New York, NY. SMC acknowledges grant funding from: (a) Together Strong-NPC Foundation. (b) National Institutes of Health, National Institute of Neurological Disorders and Stroke/National Institute on Aging R01 NS114413

Acknowledgements

We would like to thank Lauren Kalinoski, MS, CMI for her contributions to the graphical abstract.

Conflict of interest

(VKA) Patents (provisional and pending- as inventor or co-inventor), owned by the Board of Trustees of The University of Illinois.

Author contributions

KS, SMC, and HL planned experiments, performed experiments, analyzed data, and wrote the paper; DS, AB, and MA performed experiments and analyzed data; SK performed experiments; RCM planned experiments; HK and VKA planned experiments, analyzed data, and wrote the paper; DShukla analyzed data and wrote the paper.

Data accessibility

The data that support the findings of this study are available from the corresponding author upon reasonable request, and upon clearance from the University of Illinois at Chicago and/or the Veterans Affairs Administration.

References

- 1 Alon A, Schmidt HR, Wood MD, Sahn JJ, Martin SF & Kruse AC (2017) Identification of the gene that codes for the $\sigma 2$ receptor. *Proc Natl Acad Sci USA* **114**, 7160–7165.
- 2 Tesei A, Cortesi M, Zamagni A, Arienti C, Pignatta S, Zanoni M, Paolillo M, Curti D, Rui M & Rossi D (2018) Sigma receptors as endoplasmic reticulum stress “gatekeepers” and their modulators as emerging new weapons in the fight against cancer. *Front Pharmacol* **9**, 711.
- 3 Kuroda M, Fujikura D, Nanbo A, Marzi A, Noyori O, Kajihara M, Maruyama J, Matsuno K, Miyamoto H & Yoshida R (2015) Interaction between TIM-1 and NPC1 is important for cellular entry of Ebola virus. *J Virol* **89**, 6481–6493.
- 4 Mrschtik M & Ryan KM (2015) Lysosomal proteins in cell death and autophagy. *FEBS J* **282**, 1858–1870.
- 5 Pfeffer SR (2019) NPC intracellular cholesterol transporter 1 (NPC1)-mediated cholesterol export from lysosomes. *J Biol Chem* **294**, 1706–1709.
- 6 Gordon YJ, Romanowski EG & McDermott AM (2005) A review of antimicrobial peptides and their therapeutic potential as anti-infective drugs. *Curr Eye Res* **30**, 505–515.
- 7 Oudhoff MJ, Kroeze KL, Nazmi K, van den Keijbus PA, Hof W, Fernandez-Borja M, Hordijk PL, Gibbs S, Bolscher JGM & Veerman ECI (2009) Structure-activity analysis of histatin, a potent wound healing peptide

from human saliva: cyclization of histatin potentiates molar activity 1000-fold. *FASEB J* **23**, 3928–3935.

8 Oudhoff MJ, Bolscher JG, Nazmi K, Kalay H, van't Hof W, Amerongen AVN & Veerman EC (2008) Histatins are the major wound-closure stimulating factors in human saliva as identified in a cell culture assay. *FASEB J* **22**, 3805–3812.

9 Torres P, Castro M, Reyes M & Torres V (2018) Histatins, wound healing, and cell migration. *Oral Dis* **24**, 1150–1160.

10 van Dijk IA, Ferrando ML, van der Wijk A-E, Hoebe RA, Nazmi K, de Jonge WJ, Krawczyk PM, Bolscher JG, Veerman EC & Stap J (2017) Human salivary peptide histatin-1 stimulates epithelial and endothelial cell adhesion and barrier function. *FASEB J* **31**, 3922–3933.

11 van Dijk IA, Veerman EC, Reits EA, Bolscher JG & Stap J (2018) Salivary peptide histatin 1 mediated cell adhesion: a possible role in mesenchymal-epithelial transition and in pathologies. *Biol Chem* **399**, 1409–1419.

12 Jiang W-P, Wang Z, Xu L-X, Peng X & Chen F (2015) Diagnostic model of saliva peptide finger print analysis of oral squamous cell carcinoma patients using weak cation exchange magnetic beads. *Biosci Rep* **35** e00211.

13 Imamura Y, Fujigaki Y, Oomori Y, Usui S & Wang P-L (2009) Cooperation of salivary protein histatin 3 with heat shock cognate protein 70 relative to the G1/S transition in human gingival fibroblasts. *J Biol Chem* **284**, 14316–14325.

14 Imamura Y & Wang P-L (2014) Salivary histatin 3 inhibits heat shock cognate protein 70-mediated inflammatory cytokine production through toll-like receptors in human gingival fibroblasts. *J Inflamm* **11**, 4.

15 Besnard J, Ruda GF, Setola V, Abecassis K, Rodriguez RM, Huang X-P, Norval S, Sassano MF, Shin AI & Webster LA (2012) Automated design of ligands to polypharmacological profiles. *Nature* **492**, 215–220.

16 Kalmodia S, Son K-N, Cao D, Lee B-S, Surenhu B, Shah D, Ali M, Balasubramaniam A, Jain S & Aakalu VK (2019) Presence of histatin-1 in human tears and association with aqueous deficient dry eye diagnosis: a preliminary study. *Sci Rep* **9**, 1–10.

17 Ebrahimi-Fakhari D, Wahlster L, Bartz F, Werenbeck-Ueding J, Praggastis M, Zhang J, Jogerst-Thomalla B, Theiss S, Grimm D & Ory DS (2016) Reduction of TMEM97 increases NPC1 protein levels and restores cholesterol trafficking in Niemann-pick type C1 disease cells. *Hum Mol Genet* **25**, 3588–3599.

18 Qiu G, Sun W, Zou Y, Cai Z, Wang P, Lin X, Huang J, Jiang L, Ding X & Hu G (2015) RNA interference against TMEM97 inhibits cell proliferation, migration, and invasion in glioma cells. *Tumor Biology* **36**, 8231–8238.

19 Xu X-Y, Zhang L-J, Yu Y-Q, Zhang X-T, Huang W-J, Nie X-C & Song G-Q (2014) Down-regulated MAC30 expression inhibits proliferation and mobility of human gastric cancer cells. *Cell Physiol Biochem* **33**, 1359–1368.

20 Liu C-C, Yu C-F, Wang S-C, Li H-Y, Lin C-M, Wang H-H, Abate C & Chiang C-S (2019) Sigma-2 receptor/TMEM97 agonist PB221 as an alternative drug for brain tumor. *BMC Cancer* **19**, 473.

21 Zhao Z-R, Zhang L-J, He X-Q, Zhang Z-Y, Zhang F, Li F, Pei Y-B, Hu Y-M, Wang M-W & Sun X-F (2011) Significance of mRNA and protein expression of MAC30 in progression of colorectal cancer. *Chemotherapy* **57**, 394–401.

22 Xiao M, Li H, Yang S, Huang Y, Jia S, Wang H, Wang J & Li Z (2013) Expression of MAC30 protein is related to survival and clinicopathological variables in breast cancer. *J Surg Oncol* **107**, 456–462.

23 Schmit K & Michiels C (2018) TMEM proteins in cancer: a review. *Front Pharmacol* **9**, 1345.

24 Han K-Y, Gu X, Wang H-R, Liu D, Lv F-Z & Li J-N (2013) Overexpression of MAC30 is associated with poor clinical outcome in human non-small-cell lung cancer. *Tumor Biol* **34**, 821–825.

25 Ma D, Sun W, Nazmi K, Veerman EC, Bikker FJ, Jaspers RT, Bolscher JG & Wu G (2020) Salivary Histatin 1 and 2 are targeted to mitochondria and endoplasmic reticulum in human cells. *Cells* **9**, 795.

26 Vitale L, Piovesan A, Antonaros F, Strippoli P, Pelleri MC & Caracausi M (2019) Dataset of differential gene expression between total normal human thyroid and histologically normal thyroid adjacent to papillary thyroid carcinoma. *Data Brief* **24**, 103835.

27 Mohan T, Deng L & Wang B-Z (2017) CCL28 chemokine: An anchoring point bridging innate and adaptive immunity. *Int Immunopharmacol* **51**, 165–170.

28 Nakasone N, Nakamura YS, Higaki K, Oumi N, Ohno K & Ninomiya H (2014) Endoplasmic Reticulum-associated Degradation of Niemann-Pick C1 evidence for the role of heat shock proteins and identification of lysine residues that accept ubiquitin. *J Biol Chem* **289**, 19714–19725.

29 Khan SA, Fidel PL Jr, Al Thunayyan A, Varlotta S, Meiller TF & Jabra-Rizk MA (2013) Impaired histatin-5 levels and salivary antimicrobial activity against *C. albicans* in HIV infected individuals. *J AIDS Clin Res* **4**, 1000193.

30 Osuna-Ramos JF, Reyes-Ruiz JM & del Ángel RM (2018) The role of host cholesterol during flavivirus infection. *Front Cell Infect Microbiol* **8**, 388.

31 Dhara Shah MA, Shukla D, Jain S & Aakalu VK (2017) Effects of histatin-1 peptide on human corneal epithelial cells. *PLoS ONE* **12**, e0178030.

32 Roth, BL PDSP Assay Manual. <https://pdsp.unc.edu/pdspweb/>

33 Yakoub AM & Shukla D (2015) Herpes simplex virus-1 fine-tunes host's autophagic response to infection: a comprehensive analysis in productive infection models. *PLoS ONE* **10**, e0124646.

34 Duggal N, Jaishankar D, Yadavalli T, Hadigal S, Mishra YK, Adelung R & Shukla D (2017) Zinc oxide tetrapods inhibit herpes simplex virus infection of cultured corneas. *Mol Vision* **23**, 26.

35 Abdel-Naby W, Cole B, Liu A, Liu J, Wan P, Guaiquil VH, Schreiner R, Infanger D, Lawrence BD & Rosenblatt MI (2017) Silk-derived protein enhances corneal epithelial migration, adhesion, and proliferation. *Invest Ophthalmol Vis Sci* **58**, 1425–1433.

36 Riad A, Zeng C, Weng C-C, Winters H, Xu K, Makvandi M, Metz T, Carlin S & Mach RH (2018) Sigma-2 Receptor/TMEM97 and PGRMC-1 increase the rate of internalization of LDL by LDL receptor through the formation of a ternary complex. *Sci Rep* **8**, 1–12.

37 Nguyen TT, Li W, Park TJ, Gong L-W & Cologna SM (2019) Investigating phosphorylation patterns of the ion channel TRPM7 using multiple extraction and enrichment techniques reveals new phosphosites. *J Am Soc Mass Spectrom* **30**, 1359–1367.

38 Ellinger P, Kluth M, Stindt J, Smits SH & Schmitt L (2013) Detergent screening and purification of the human liver ABC transporters BSEP (ABCB11) and MDR3 (ABCB4) expressed in the yeast *Pichia pastoris*. *PLoS ONE* **8**, e60620.

39 Rouse SL, Marcoux J, Robinson CV & Sansom MS (2013) Dodecyl maltoside protects membrane proteins in vacuo. *Biophys J* **105**, 648–656.

40 Siligardi G, Hussain R, Patching SG & Phillips-Jones MK (2014) Ligand-and drug-binding studies of membrane proteins revealed through circular dichroism spectroscopy. *Biochim Biophys Acta* **1838**, 34–42.

41 Wang X, Kamiyama K, Iguchi I, Kita M & Imanishi J (1994) Enhancement of fibronectin-induced migration of corneal epithelial cells by cytokines. *Invest Ophthalmol Vis Sci* **35**, 4001–4007.

Supporting information

Additional supporting information may be found online in the Supporting Information section at the end of the article.

Fig. S1. Hst1 coimmunoprecipitates with TMEM97.

Fig. S2. Analysis of binding of Hst1 with TMEM97 using ELISA.

Fig. S3. Surface plasmon resonance (SPR) analysis.

Fig. S4. Pretreatment of cells with DTG blocks Hst1 internalization and localization.

Fig. S5. siRNA-mediated KD of TMEM97 in HCE cells indicates necessity of TMEM97 for Hst1 effects on wound healing rates.